w/ errata !!!

Gaussian beam tracing for computing ocean acoustic fields

Michael B. Porter
Naval Research Laboratory, Washington, DC 20375

Homer P. Bucker
Naval Ocean Systems Center, San Diego, California 92152

(Received 29 December 1986; accepted for publication 30 June 1987)

The method of Gaussian beam tracing has recently received a great deal of attention in the seismological community. In comparison to standard ray tracing, the method has the advantage of being free of certain ray-tracing artifacts such as perfect shadows and infinitely high energy at caustics. It also obviates the need for eigenray computations. The technique is especially attractive for high-frequency, range-dependent problems where normal mode, FFP, or parabolic models are not practical alternatives. The Gaussian beam method associates with each ray a beam with a Gaussian intensity profile normal to the ray. The beamwidth and curvature are governed by an additional pair of differential equations, which are integrated along with the usual ray equations to compute the beam field in the vicinity of the central ray of the beam. We have adapted the beam-tracing method to the typical ocean acoustic problem of a point source in a cylindrically symmetric waveguide with depth-dependent sound speed. We present an overview of the method and a comparison of results obtained by conventional ray-tracing, beam-tracing, and full-wave theories. These results suggest that beam tracing is markedly superior to conventional ray tracing.

PACS numbers: 43.30.Cq, 43.30.Dr

INTRODUCTION

Beam tracing has recently received a great deal of attention for solving problems in wave propagation.[1–27] In particular, the seismological literature includes a large number of references. Basically, the method consists of approximating a given source by a fan of beams and tracing the propagation of these beams through the medium. The quantities of interest, e.g., acoustic pressure or particle displacement, are then computed at a specified location by summing the contributions of each of the individual beams.

The behavior of individual beams is a classical problem in physics. However, the recent literature is concerned with the propagation of waves from point or line sources and a fan of bounded beams is simply used to approximate the source. Thus although bounded beams occur quite naturally in acoustics the technique is generally applicable to sources that are not "beamlike." Indeed, for our test problems we consider the standard ocean acoustics problem of a point source in cylindrical coordinates.

Less formal beam theories have been applied previously to ocean acoustic problems. Perhaps the simplest procedure involves a user specified and range-independent beamwidth (interpreted as representing the diffusivity of a ray due to statistical fluctuations). This kind of procedure has been implemented in several ray models. More recently, Bucker developed a beam theory based on spreading laws in a homogeneous medium, which allowed the beams to evolve as arc length increased. The present theory employs differential equations that are integrated along with the usual ray equations and that govern the evolution of both the beam curvature and width. Initial results of this theory and comparisons with Bucker's simple Gaussian beam theory were presented in Ref. 23.

The standard ray-tracing method produces certain artifacts, e.g., perfect shadows and caustics. Extended ray theories have been developed in order to correct for these difficulties; however, these algorithms tend to be awkward to implement. In contrast, beam tracing requires only simple modifications to standard ray-tracing codes and the solutions so generated are free of singularities at caustics and abrupt discontinuities at shadow zone boundaries. In addition, the beam approach obviates the need for time-consuming and failure-prone eigenray computations.

In the following sections we review the beam-tracing technique and discuss the modifications required to apply it to ocean acoustic problems in cylindrical coordinates. We describe the practical aspects of its implementation and compare the performance of the method to conventional ray tracing for several different scenarios.

I. REVIEW OF THE GAUSSIAN BEAM EQUATIONS

A readable introduction to Gaussian beam tracing along with an historical overview including references to the earliest works is provided by Cerveny *et al.*[12] Basically, the construction begins with the integration of the usual ray equations to obtain the central ray of the beam. Beams are then constructed about the rays by integrating a pair of auxiliary equations, which govern the evolution of the beam in terms of the beamwidth and curvature as a function of arc length. The resulting pressure field describes a beam, in that the field falls off in a Gaussian fashion as a function of normal distance from the central ray of the beam.

The central ray of the beam obeys the standard ray equations. We consider a cylindrical coordinate system with r denoting the horizontal range and z the depth coordinate. The ray equations then read

 0001-4966/87/101349-11$00.80

$$\frac{d}{ds}\left(\frac{1}{c(r,z)}\frac{d\mathbf{r}}{ds}\right) = -\frac{1}{c^2(r,z)}\nabla c(r,z)\,,$$

where $\mathbf{r} = \mathbf{r}(s)$, the $[r(s),z(s)]$ coordinate of the ray as a function of the arc length s, and $c(r,z)$ is the sound speed. These equations may be immediately reduced to first-order form by introducing the auxiliary variables (ρ,ζ). This is convenient since numerical integrators for initial value problems are often stated for first-order systems. In addition, $[\rho(s),\zeta(s)]$ is proportional to the local tangent vector, which turns out to be a useful quantity. In first-order form, the ray equations then read

$$\frac{dr}{ds} = c\rho(s)\,, \tag{1a}$$

$$\frac{d\rho}{ds} = -\frac{1}{c^2}\frac{\partial c}{\partial r}\,, \tag{1b}$$

$$\frac{dz}{ds} = c\zeta(s)\,, \tag{1c}$$

$$\frac{d\zeta}{ds} = -\frac{1}{c^2}\frac{\partial c}{\partial z}\,. \tag{1d}$$

The beam curvature and width are derived from the quantities $p(s)$ and $q(s)$, which are obtained by integrating an additional pair of ordinary differential equations along the central ray. These additional equations are derived by solving a parabolic equation in the neighborhood of each ray. The details of this derivation are given in Appendix A and we present only the final result here:

$$\frac{dq}{ds} = c(s)p(s)\,, \tag{2a}$$

$$\frac{dp}{ds} = -\frac{c_{nn}}{c^2(s)}q(s)\,. \tag{2b}$$

Here, c_{nn} denotes the second normal derivative of the sound speed $c(r,z)$ and may be computed as

$$\begin{aligned} c_{nn} &= c_{rr}\left(\frac{dr}{dn}\right)^2 + 2c_{rz}\left(\frac{dr}{dn}\right)\left(\frac{dz}{dn}\right) + c_{zz}\left(\frac{dz}{dn}\right)^2 \\ &= c_{rr}(N_{(r)})^2 + 2c_{rz}(N_{(r)})(N_{(z)}) + c_{zz}(N_{(z)})^2\,, \end{aligned} \tag{3}$$

where $(N_{(r)}, N_{(z)})$ is a unit normal given by

$$(N_{(r)},N_{(z)}) = \left(\frac{dz}{ds}, -\frac{dr}{ds}\right) = c(S)[\zeta(s), -\rho(s)]\,. \tag{4}$$

The beam is then defined by

$$\begin{aligned} u(s,n) = A&\sqrt{c(s)/[rq(s)]} \\ &\times\exp(-i\omega\{\tau(s) + 0.5[p(s)/q(s)]n^2\})\,, \end{aligned} \tag{5}$$

where A is an arbitrary constant, n is the normal distance from the central ray, and ω is the angular frequency of the source. We observe that this form differs from the result of Cerveny *et al.*[12] by a factor of $\sqrt{r}$ that represents the effect of cylindrical spreading.

The term $\tau(s)$ in (5) is the phase delay (travel time) that satisfies

$$\frac{d\tau}{ds} = \frac{1}{c(s)}\,. \tag{6}$$

In order for Eq. (5) to be a complete description of the beam field, we must specify the intended branch of the square root. The branch is chosen so that the resulting phase varies continuously with the arc length s. Thus the square root is defined by

$$\sqrt{x} = (-1)^{m(s)}\,\mathrm{sqrt}(x)\,, \tag{7}$$

where $\mathrm{sqrt}(x)$ now denotes the principal value, i.e., the branch of the square root that yields a resulting phase in $(-\pi/2,\pi/2)$. The function $m(s)$ is the integer number giving the number of times $c(s)/[rq(s)]$ [or equivalently $q(s)$] has crossed the negative imaginary axis and is easily computed during the integration of the p–q equations.

II. INITIAL CONDITIONS

The initial conditions for the system of four ordinary differential equations governing the central ray of the beam are

$$\begin{aligned} &[r(0),z(0)] = (r_s,z_s)\,, \\ &[\rho(0),\zeta(0)] = (\cos\alpha, \sin\alpha)/c(0)\,, \end{aligned} \tag{8}$$

where (r_s,z_s) denotes the source location and α is a prescribed takeoff angle. We measure angles with respect to the horizontal r axis and use positive angles for downgoing rays so that α is a declination angle.

In order to discuss the p–q initial conditions, it is convenient to relate the p–q functions to a beam radius (half-width) $L(s)$,and beam curvature $K(s)$. These functions are defined by

$$\begin{aligned} L(s) &= \sqrt{-2/\{\omega\,\mathrm{Im}[p(s)/q(s)]\}}\,, \\ K(s) &= -c(s)\mathrm{Re}[p(s)/q(s)]\,. \end{aligned} \tag{9}$$

Plainly, the beam radius $L(s)$ is the normal distance from the central ray at which the beam amplitude is $1/e$ of its maximum value. Furthermore, if the wave fronts are curved, then traveling normal to the central ray corresponds to traversing curves of constant phase. The rate of change of phase relates directly to the local curvature and provides the basis for the interpretation of $K(s)$ as curvature.[28]

At present there is no consensus on the proper choice of $p(0)$ and $q(0)$, or equivalently, $L(0)$ and $K(0)$. Cerveny *et al.*,[12] chose initial conditions so as to minimize the beam-width at the receiver. The guiding principle for this choice is that the computation time may be reduced if the number of contributing beams is minimized. One complication of this approach is that if the beams are individually made to have minimum width, then each beam will in general have a different initial beam constant and the expansion of a point source into beams must be re-examined. (Muller[21] has addressed this issue and argued that Cerveny's *et al.*,[12] original expansion procedure is not significantly degraded when the beam parameter is nonconstant.)

Numerous other choices have been considered, such as minimizing beamwidth at the source or the midpoint between source and receiver; Madariaga[22] argues that initial

conditions should not differ too much from those that correspond to WKB theory.

We have been able to obtain good results, for the cases considered so far, by assuming that the beam is initially flat (no curvature) and choosing the initial beamwidth so that the beams are "space filling" in the farfield. In order to obtain an initially flat beam, $q(0)$ is set to an imaginary constant of magnitude ϵ:

$$p(0) = 1, \quad q(0) = i\epsilon . \tag{10}$$

Note that since p occurs in Eq. (2) only as the quotient (p/q), we can choose $p(0) = 1$ without loss of generality. Then referring to Eq. (9), we see that purely real ϵ is equivalent to zero curvature beams.

We next select ϵ to obtain a "space-filling" beam in the farfield. Consider the canonical problem of a beam in a homogeneous medium with constant sound speed c_0 equal to that at the source location in the original problem. In a homogeneous medium the p–q equations are readily solved to yield

$$p(s) = 1, \quad q(s) = c_0 s + i\epsilon \tag{11}$$

or

$$p(s)/q(s) = (c_0 s - i\epsilon)/(c_0^2 s^2 + \epsilon^2) . \tag{12}$$

Therefore, the beam defined by Eq. (5) falls off with n (the normal distance from the central ray) according to

$$\exp[\, -0.5\omega\epsilon n^2/(c_0^2 s^2 + \epsilon^2)\,] . \tag{13}$$

Now, if a fan of N beams is traced over an angular spread (α_1, α_2), then each beam "occupies" an angle of $\delta\alpha = (\alpha_2 - \alpha_1)/(N-1)$ and the normal distance to the central ray of a neighboring beam is given by $n = s\delta\alpha$. For reasonable coverage at long ranges ($c_0 s \gg \epsilon$), we then choose ϵ such that the beam influence is reduced by $1/e$ at the location of its two neighboring beams. Therefore,

$$\epsilon = 2c_0^2/[\omega(\delta\alpha)^2] , \tag{14}$$

which together with Eq. (10) completes the specification of the p–q initial conditions.

In our test problems these initial conditions have always yielded better results than ray tracing; however, we find that still better results may be obtained by adjusting the initial conditions. Ultimately, we expect that better guidelines will emerge for choosing the p–q initial conditions.

III. EXPANSION OF A POINT SOURCE INTO BEAMS

For sources that naturally give rise to a beam solution, a single beam may be used to approximate the source and the expansion is immediate. In many cases, however, the sources are not "beamlike" and the issue of how to approximate the source as a superposition of beams must be addressed. One approach is to match the high-frequency asymptotic field of the Gaussian beam representation to the exact solution in a homogeneous medium. Thus, following Cerveny *et al.*,[12] we seek an expansion of the field as an integral over the beam takeoff angle:

$$u(\alpha_0) = \int A(\alpha) \sqrt{\frac{c(s)}{rq(s)}} \times \exp\left\{ -i\omega\left[\tau + 0.5\left(\frac{p}{q}\right)n^2\right]\right\} d\alpha , \tag{15}$$

where α_0 denotes the angle to the receiver. In a homogeneous medium, formulas for $p(s)$, $q(s)$, and $\tau(s)$ may all be obtained easily. The analysis of Cerveny *et al.*[12] carries through directly, with appropriate sign changes and the factor of $1/\sqrt{r}$ carried through. The saddle point method yields the high-frequency asymptotic approximation:

$$u(\alpha_0) \sim A(\alpha_0) c_0 \sqrt{2\pi/[q(0)\omega r R\,]} \times \exp(\, -i\omega R/c_0 - i\pi/4) , \tag{16}$$

where R is the slant range to the receiver and r is the (r,z) cylindrical coordinate of the receiver. The quantity $q(0)$ denotes the initial value of q and is given by Eq. (10).

It is convenient to convert the entire expression to (R,z) coordinates using $r = R\cos\alpha_0$. Then one may match to the exact solution for a point source in three dimensions:

$$u(R) = \exp(\, -i\omega R/c_0)/R . \tag{17}$$

Evidently the forms will match if

$$A(\alpha) = (1/c_0)\exp(i\pi/4)\sqrt{q(0)\omega\cos\alpha/(2\pi)} , \tag{18}$$

and so the beam field is constructed as

$$u(\alpha_0) = \sum \delta\alpha \left(\frac{1}{c_0}\right) \exp\left(\frac{i\pi}{4}\right) \sqrt{\frac{q(0)\omega\cos\alpha}{2\pi}} \times \sqrt{\frac{c(s)}{rq(s)}} \exp\left\{ -i\omega\left[\tau + 0.5\left(\frac{p}{q}\right)n^2\right]\right\} , \tag{19}$$

where the integral sign has been replaced by a discrete approximation to the integral. The final result differs from the expansion of a line source[12] by a factor of $1/\sqrt{r}$ in range, $\cos\alpha$ angular weighting, and by a multiplicative constant.

IV. REFLECTION AND TRANSMISSION AT INTERFACES

Cerveny and Psencik[17] provide complete equations for beam transmission/reflection through a first-order curved acoustic interface. The transmission/reflection equations are derived by matching the phase of the incident and transmitted beams at the interface. (Felsen[18] has argued that the reflection and transmission coefficients of Cerveny and Psencik[17] should employ the complex angle of incidence of an associated complex ray rather than the real angle of incidence of the central ray of the beam. This is an effect that presumably would be included if the matching had been carried through to the amplitude equation.)

In our test problems, we consider range-independent problems and the only interface is the ocean surface. This is a weak or second-order interface in that the sound speed is continuous, but its higher-order derivatives are not. The reflection formulas at the interface may then be simplified considerably and one obtains

$$r' = r, \quad \rho' = \rho , \tag{20a}$$

$$z' = z, \quad \zeta' = -\zeta, \tag{20b}$$

$$p' = p + qN, \quad q' = q, \tag{20c}$$

$$\tau' = \tau - (\pi/\omega), \tag{20d}$$

where

$$N = 2\rho[c_r(2\zeta - \rho^2/\zeta) - c_z\rho]/(\zeta c)\big|_{z=0}.$$

Here, primes refer to the variable values after reflecting from the interface. Equations (20a) and (20b) assert that the beam reflects from the surface at the same position it enters and with the same angle. In addition, Eqs. (20c) imply

$$p'/q' = p/q + N, \tag{21}$$

where N is real. Since the imaginary part of p/q governs the beamwidth and the real part the beam curvature, one concludes that the beam undergoes no change in width but does change its curvature. Finally, Eq. (20d) accounts for the phase shift during reflection.

A shortcoming of Eqs. (20) is that they are not valid near grazing incidence. One finds that the contributions of "adjacent" beams to a particular receiver are out of phase for beams near grazing incidence and that the resulting pressure field is incorrect. In the range-independent problems that we consider here, we have found empirically that the following formula corrects for this deficiency:

$$N = 4(c_z/c)\rho^2/\zeta\big|_{z=0}. \tag{22}$$

A more complete treatment of reflected beams near grazing incidence is deferred to a future paper.

V. PRACTICAL COMPUTATIONAL ASPECTS

The tracing of an individual beam involves the classical problem of integrating a set of coupled nonlinear ordinary differential equations. In wave propagation problems the methods employed may be divided into two classes—conventional integration methods and patch methods. In the first class we include Runge–Kutta and multistep methods, which are part of standard packages. In patch methods, the domain of the problem is divided into subdomains in which the material properties are approximated by simple analytical forms. The forms are chosen so that the differential equations may be solved analytically within each patch or subdomain. In two (three) dimensions one may divide the domain into triangles (tetrahedra) with linearly varying sound speed or square index of refraction. Within these subdomains exact solutions for the rays are obtained as parabolas or arcs of circles depending on the particular approximation.

The different approaches manifest different features or problems. In the final analysis the difference between the quality of individual codes probably depends more on the craft of the programmer than on the class of solver used and at this time, there is no clear choice between the two approaches. Happily, the Gaussian beam approach is easily imbedded in either type of code. In order to employ patch methods, it is necessary to construct analytic solutions for the beam equations. The two most popular cases employ linear approximations to $c(r,z)$ or $n^2(r,z)$, where n is the index of refraction. The equations for the central ray of the beam are just the usual ray equations and yield ray paths that are circles and parabolas, respectively. In order to complete the beam solution it is also necessary to solve the p–q equations analytically. The c-linear case is trivially integrable and has been treated in detail elsewhere.[21] The n^2-linear case seems to have been preferred in ocean acoustics problems and analytic solutions to the p–q equations may also be obtained for this case. The relevant formulas are presented in Appendix B.

For test purposes we have employed the "improved polygon method,"[29] which for a system $y' = f(x,y)$ yields the discretization

$$\begin{aligned} y(i+1/2) &= y(i) + (h/2)f[x(i),y(i)], \\ y(i+1) &= y(i) + hf[x(i+1/2),y(i+1/2)], \end{aligned} \tag{23}$$

where h is the step length and $x(i), y(i)$ denotes the values of x and y obtained at the ith step. In a production code, a more sophisticated integrator such as Runge–Kutta–Fehlberg is probably more suitable.

We trace a fan of these beams using an angular spread and total arc length for each beam so as to obtain all beams that might contribute to a specified receiver point. The treatment of the next step depends on the kind of computation desired (complete field, just along a fixed depth, or range, etc.) and on the method of integration. In our case, we are interested in computing propagation loss along a receiver track at a fixed depth z_r and extending over a series of discrete range coordinates, $(r_l,\ l = 1,\ldots)$. A beam is traced and at each step we compute the intercept of ray normal and the receiver line. We then identify the receivers lying between successive ray normal intercepts and compute the contribution of the beam field at each receiver by interpolation.

The interpolation of the beam solution between tabulated points on the beam may be performed in a variety of ways. Cerveny *et al.*[12] construct a family of normals to the line segment connecting two adjacent points on the beam. They then determine the particular normal that passes through the receiver point and use linear interpolation to compute the beam influence. A drawback of this approach is that it leaves wedge-shaped regions extending from each of the tabulated points in which no normal connects a receiver and the polygon train of the central ray.

We have employed an alternative approach, which makes use of the fact that $(N_{(r)}, N_{(z)}) = c(s_j)[(\zeta(s_j),\rho(s_j)]$ is the beam normal at each node during the integration process. Then, the r coordinate of the point where the normal intercepts the receiver line is given by

$$r_{\text{int}} = r(s_j) + [z_r - z(s_j)]N_{(r)}/N_{(z)}. \tag{24}$$

By construction, the receiver point is bracketed by the intercept points of two adjacent normals, which we denote by r_a and r_b. Therefore, we may define the proportional distance of the receiver point along this segment by

$$w = (r_{\text{int}} - r_a)/(r_b - r_a) \tag{25}$$

and an arbitrary quantity f on the beam is obtained by linear interpolation, $f = (1-w)f(a) + wf(b)$. Linear interpolation is used for the quantities $n(s), p(s), q(s)$, and $\tau(s)$, which are required to construct the beam field at the receiver.

Computation time may be reduced by windowing the beam, i.e., only computing the beam influence when the beam is close to a receiver. We currently use a criterion that allows a beam to contribute if it is within five beam radii of the receiver.

This windowing was demonstrated to have no visible effect on the transmission loss plots.

VI. APPLICATIONS

The test cases considered in this section and the various input parameters are summarized in Table I. As a first example of the method, we have treated a strong downward refracting profile first considered by Pedersen and Gordon.[30] In order to avoid confusion, we have retained the original nonmetric units. The sound speed is an n^2-linear range-independent form:

$$c(z) = c_0/\sqrt{1 - 2\gamma z/c_0}, \tag{26}$$

where

$$c_0 = 1677.3319 \text{ yards/s}, \quad \gamma = -1.2286762/\text{s}.$$

A plot of this profile is shown in Fig. 1. Following Pedersen and Gordon,[30] propagation loss is calculated for a 2000-Hz source frequency and for two source/receiver combinations. In the first case both the source and receiver are located at a depth of 66.7 yards. For convenience, we reproduce the ray trace for this scenario in Fig. 2. Evidently, there is a shadow zone that begins at a range of approximately 800 yards and is manifest in the resulting ray transmission loss calculations shown in Fig. 3(a).

A reference solution for this problem is readily obtained from the plane-wave spectral integral. The result, shown in Fig. 3(b), was obtained by the Kutschale[31]–Wales "fast field program," which employs the Airy function solution for n^2-linear layers. For this particular problem, which is composed of a single n^2-linear half-space, one layer suffices. Not surprisingly, the full-wave solution has a much less abrupt transition at the shadow zone boundary. The beam trace results shown in Fig. 3(c) are much more faithful to the reference solution replicating the smooth transition to the shadow zone.

In the second case the source is located at a depth of 1000 yards and a receiver track is located at a depth of 800 yards. A ray trace is shown in Fig. 4. As discussed by Pedersen and Gordon,[30] this track passes through three successive zones as range increases. In the nearfield the interference pattern is due to the interaction of a surface reflected and a direct refracted arrival. At a range of approximately 3130 yards the surface reflected ray is turned before reaching the surface and the interference is between two direct arrivals. Finally, at a distance of approximately 3160 yards a caustic is found and beyond that a shadow zone where ray theory predicts zero amplitude. For comparison, we reproduce the conventional ray-trace propagation loss curve for this scenario [Fig. 5(a)]. The transitions between each of these zones are clearly visible in this plot. Again the reference (spectral integral) solution in Fig. 5(b) shows energy diffracted into the shadow region and generally has less sharp transitions than the ray-trace solution.

In Fig. 5(c) we display the Gaussian beam propagation loss curve, which again is in extremely good agreement with the exact solution. We note that the correct caustic phase shift has

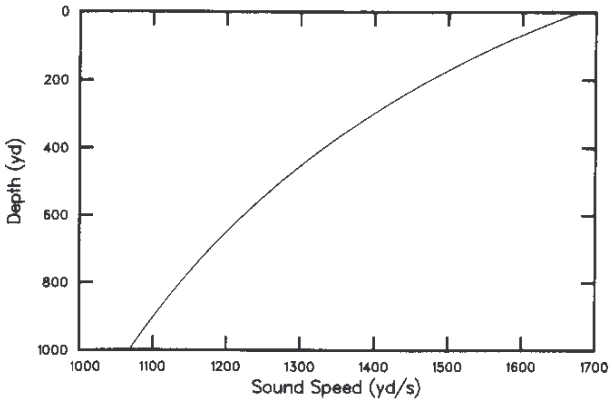

FIG. 1. Sound-speed profile for downward refracting case.

TABLE I. Summary of test problems and input parameters.

Downward refracting scenario:

$c(z) = c_0/\sqrt{(1 - 2\gamma z/c_0)}$
$c_0 = 1677.3319$ yards/s, $\gamma = -1.2286762$/s

Shallow source case:

Source depth = 66.7 yards, receiver depth = 66.7 yards
Frequency = 2000.0 Hz
101 beams distributed over (− 25.0, 0.0) degrees
200 integration steps of 10 yards per beam
501 transmission loss points over (500.0, 1000.0) yards
CPU time ≈ 100 s

Deep source case:

Source depth = 1000.0 yards, receiver depth = 800.0 yards
Frequency = 2000.0 Hz
401 beams distributed over (− 60.0, − 20.0) degrees
281 transmission loss points over (3100.0, 3170.0) yards
CPU time = 330 s

Munk profile:

$c(z) = 1500\{1.0 + 0.00737[x - 1 + \exp(-x)]\}$, for $z < 5000$ m,
$c(z) = c(5000)$, for $z > 5000$ m,
$x = 2(z - 1300)/1300$.

Source depth = 1000.0 m, receiver depth = 800.0 m
Frequency = 50.0 Hz
88 beams distributed over (− 14.66, 14.66) degrees
800 integration steps of 200 m per beam
800 transmission loss points over (0.25, 100 000.0) m
CPU time ≈ 130 s

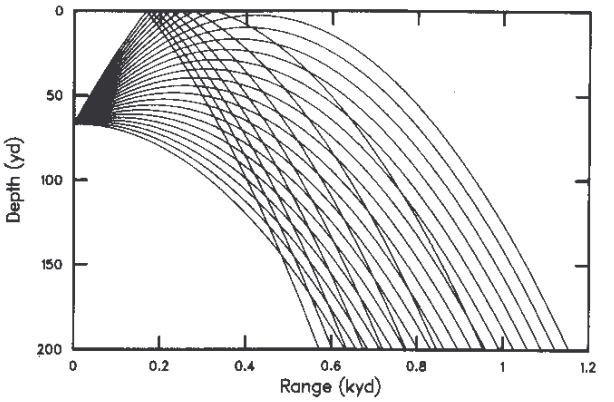

FIG. 2. Ray trace for shallow source (66.7 yards) downward-refracting profile.

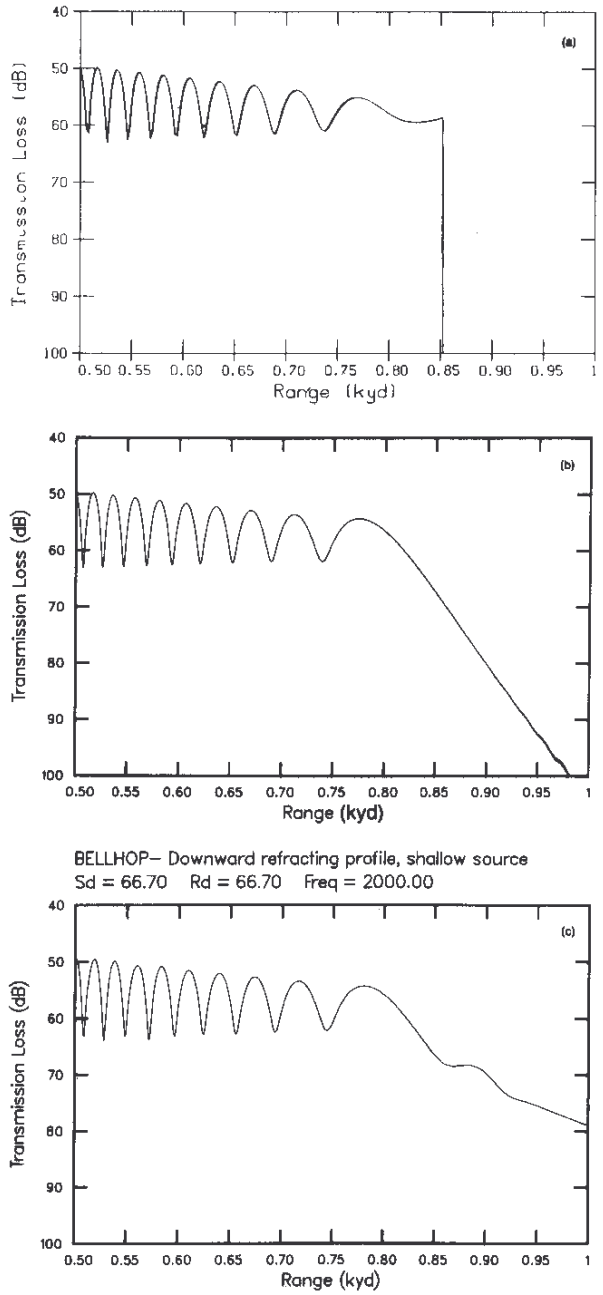

FIG. 3. (a) Ray theory propagation loss for shallow source. (b) FFP propagation loss for shallow source. (c) Gaussian beam-trace propagation loss for shallow source.

been included automatically by the beam-trace code (neglecting the phase shift causes an immediately visible shift in the inteference pattern). This phase shift is often neglected in general ray-trace codes since it requires the location of caustics. However, Fig. 5(a) employs the analytical ray solution for this profile and is thus free of many problems that might afflict a production code.

As a third example, we consider Munk's[32] canonical deep-water, sound-speed profile, where

$$c(z) = 1500\,\{1.0 + 0.00737\,[x - 1 + \exp(-x)]\}, \quad \text{for } z \leqslant 5000 \text{ m}, \quad (27)$$

$$c(z) = c(5000), \quad \text{for } z > 5000 \text{ m},$$

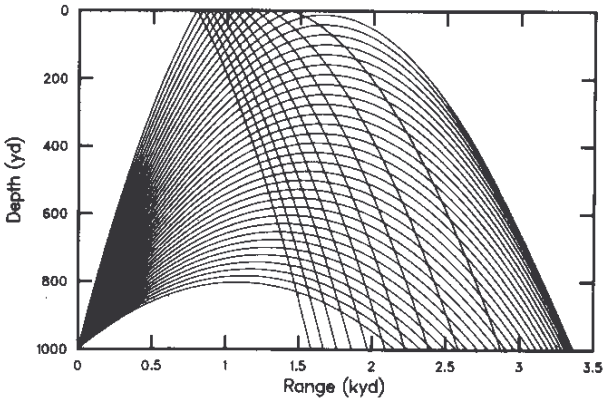

FIG. 4. Ray trace for deep source (1000 yards) downward-refracting profile.

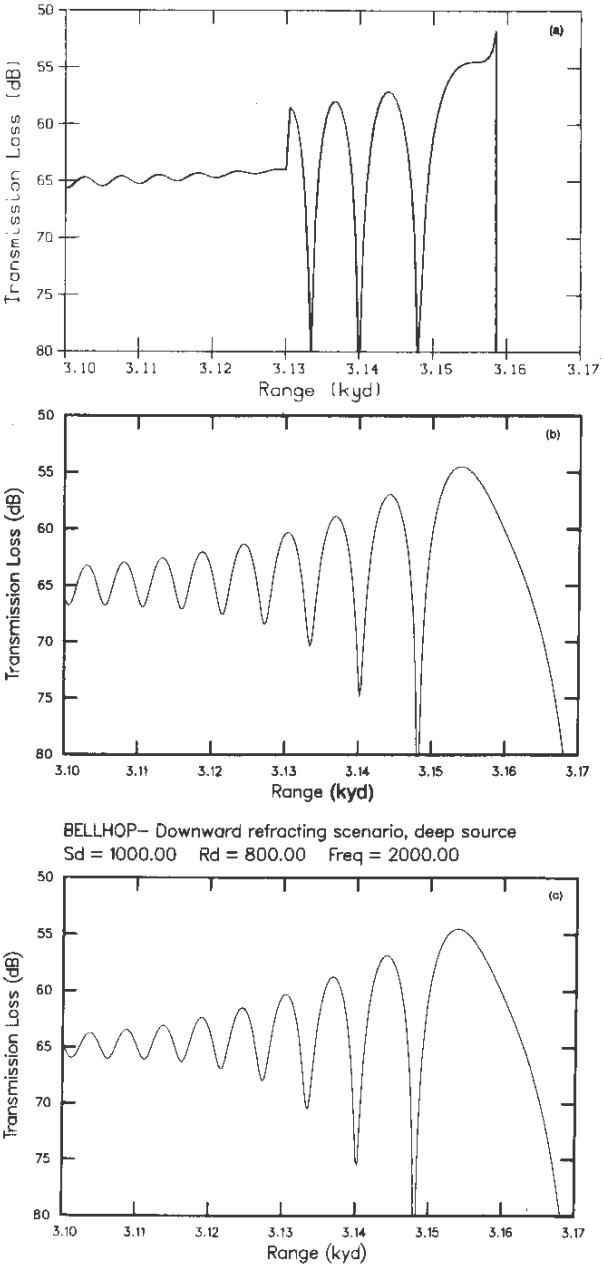

FIG. 5. (a) Ray theory propagation loss for deep source. (b) FFP propagation loss for deep source. (c) Gaussian beam-trace propagation loss for deep source.

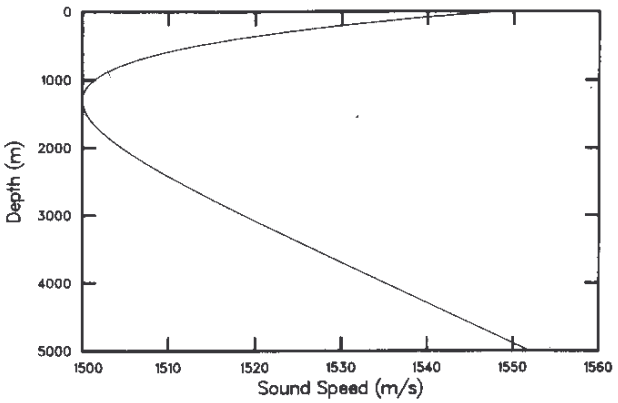

FIG. 6. Munk sound-speed profile.

with

$$x = 2(z - 1300)/1300 .$$

A sound-speed plot and ray trace for a 1000-m source are shown in Figs. 6 and 7, respectively. Since our beam-trace code does not at present allow for bottom reflection we have restricted the angular spread in all programs such that only water borne rays are included. Propagation loss is computed along a receiver track located at a depth of 800 m and extending from the source out to 100 km. The source frequency has been reduced to 50 Hz in order to facilitate comparison with a full-wave model and to demonstrate the performance at lower frequencies. This particular source depth leads to a complicated field structure including caustics and shadow zones, which as usual manifest themselves in the ray-trace propagation loss curve of Fig. 8(a) as regions of infinite and zero pressure, respectively. We see an additional fault in the form of a dropout at a range of approximately 5 km. This stems from the fact that the ray results were obtained by a production ray code that failed to identify a pair of ray paths bracketing the receiver point in range and therefore was unable to compute the ray field at that point. While this particular problem of identifying eigenrays is not intrinsic to ray codes it should be noted that it is typical.

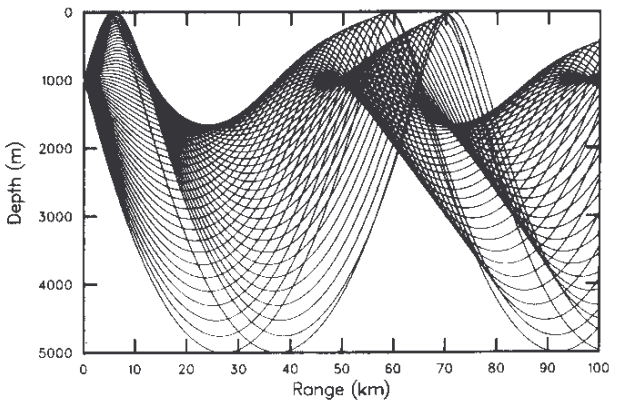

FIG. 7. Ray trace for source at 1000-m depth.

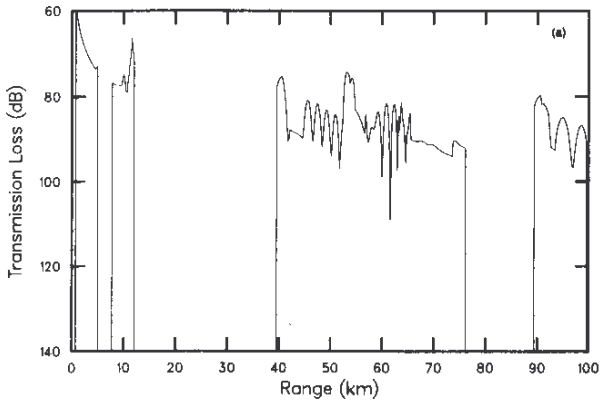

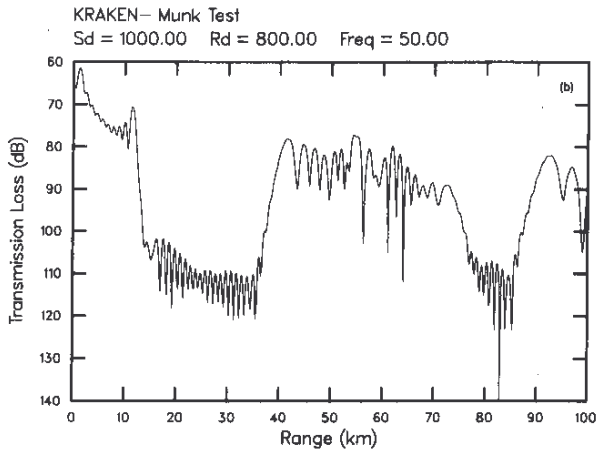

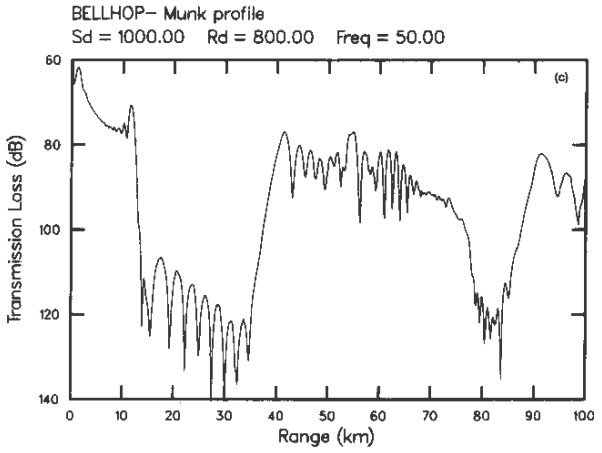

FIG. 8. (a) Ray theory propagation loss for Munk profile. (b) Normal mode propagation loss for Munk profile. (c) Gaussian beam propagation loss for Munk profile.

The Gaussian beam loss curve is shown in Fig. 8(c) and, as before, corresponds much more closely to the reference solution of Fig. 8(b) throughout the entire 100-km receiver track. The Gaussian beam solution was obtained using three beams per degree (88 beams) and required 130 s of CPU time on a VAX11/750. The reference solution was obtained by the

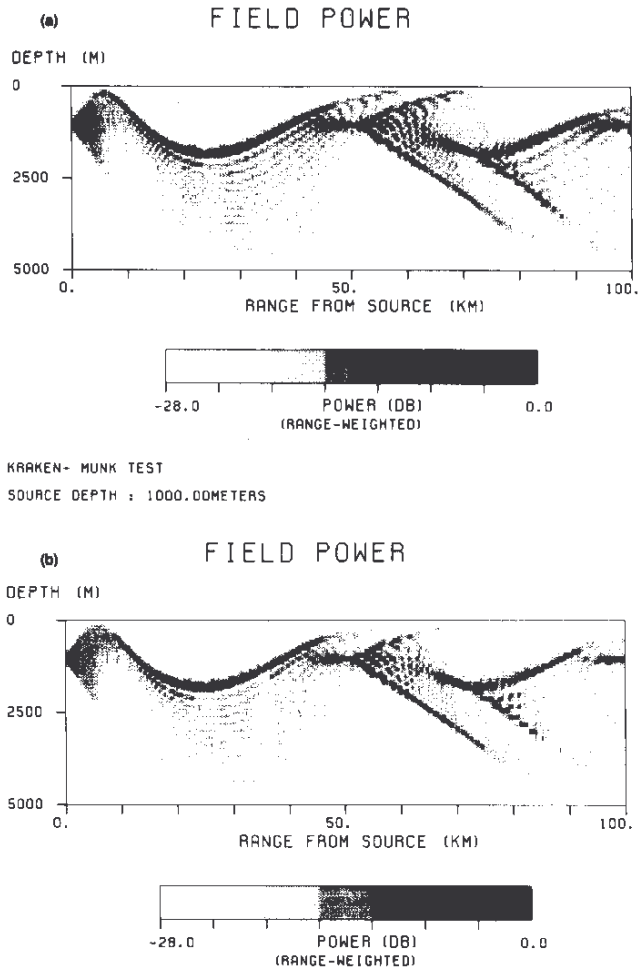

FIG. 9. (a) Normal mode propagation loss for Munk profile. (b) Gaussian beam propagation loss for Munk profile.

KRAKEN normal mode program[33] by including only those modes with phase velocity less than the half-space velocity.

Finally, in Fig. 9 we include the gray shade plot of transmission loss computed throughout the water column. (The transmission loss is multiplied by a factor of $\sqrt{r}$ to compensate approximately for cylindrical spreading.) Figure 9(a) was obtained using Gaussian beam tracing and Fig. 9(b) by using the normal mode program. We note that the agreement is excellent throughout the water column.

VII. SUMMARY

In summary, the Gaussian beam approach appears to be a very promising alternative to conventional ray tracing. In our test problems it has generated much more accurate answers than the ray solution. Although it requires slightly more effort to integrate the beam equations than the ray equations, this is compensated for by the fact that eigenray or two-point ray computations are not required and a beam trace code may well run faster than a similar implementation of ray tracing. Additional work is indicated to formally treat beams incident at critical or grazing angles and to carefully assess the merit of rules used for choosing beam initial conditions.

APPENDIX A: DERIVATION OF THE BEAM EQUATIONS

Cerveny *et al.*[12] provide a derivation of the beam equations for a line source in three dimensions. We follow closely their derivation with modifications to accomodate a point source. We begin with the Helmholtz equation governing the pressure due to a monochromatic point source:

$$\nabla^2 u + \omega^2 u = 0 . \tag{A1}$$

Our objective is to construct a solution about each ray that has the character of a beam. For any particular ray we introduce a ray-centered coordinate system (s, n), where s is the arc length along the ray and n is the normal distance from the ray. The (s, n) coordinate system is regular in some neighborhood of the ray and constitutes an orthogonal curvilinear coordinate system. The scale factors[34] of the transformation are

$$(h_s, h_n, h_\theta) = (h, 1, r) ,$$

where

$$h = 1 + (c_n/c)n .$$

Thus the Helmholtz equation is (s,n) coordinates reads

$$\begin{aligned}\nabla^2 u + \frac{\omega^2}{c^2} u &= \frac{1}{hr}\left\{\left[\left(\frac{r}{h}\right) u_s\right]_s + (hru_n)_n\right\} + \frac{\omega^2}{c^2} u \\ &= \frac{1}{h} u_{ss} + h u_{nn} + h\frac{\omega^2}{c^2} u + \left(\frac{1}{h}\right)_s u_s \\ &\quad + h_n u_n + \frac{r_s}{rh} u_s + \frac{r_n}{r} h u_n . \end{aligned} \tag{A2}$$

We next employ the parabolic substitution

$$u(s,n) = U(s,n)\exp[-i\omega\tau(s)], \quad \tau(s) = \int \frac{1}{c(s)}\, ds . \tag{A3}$$

This yields

$$\begin{aligned}&\frac{1}{h}\left\{\left[-\frac{\omega^2}{c^2} - i\omega\left(\frac{1}{c}\right)_s\right] U - 2i\frac{\omega}{c} U_s + U_{ss}\right\} \\ &\quad + hU_{nn} + h\frac{\omega^2}{c^2(s,n)} U \\ &\quad + \left(U_s - \frac{i\omega}{c} U\right)\left(\frac{1}{h}\right)_s + h_n U_n + \frac{r_s}{rh}\left(U_s - \frac{i\omega}{c} U\right) \\ &\quad + (r_n/r)\, hU_n = 0 . \end{aligned} \tag{A4}$$

The parabolic substitution involves $c(s) = c(s,n=0)$, so that Eq. (A4) involves both $c(s)$ and $c(s,n)$. We use the notation that c denotes $c(s)$, while $c(s,n)$ is used to explicitly indicate variation in (s,n) whenever both dependencies exist. We

next introduce a stretching of the normal coordinate $\nu = \omega^{1/2} n$ and collect terms of like power in ω:

$$\omega^2 h\left(\frac{1}{c^2(s,n)} - \frac{1}{h^2 c^2}\right) U + \omega\left[\frac{ic_s}{(hc^2)} U - \frac{i}{c}\left(\frac{1}{h}\right)_s U - \frac{2i}{hc} U_s + hU_{\nu\nu} - \frac{ir_s}{rhc} U\right] + \omega^{1/2}\left(U_\nu h_n + \frac{r_n h}{r} U_\nu\right) + \frac{1}{h} U_{ss} + U_s\left(\frac{1}{h}\right)_s + \frac{r_s}{rh} U_s = 0 . \quad \text{(A5)}$$

Note that no approximations have been made up to this point, so that Eq. (A5) corresponds exactly to the Helmholtz equation. Now,

$$\frac{1}{c^2(s,n)} = \frac{1}{c^2(s)} - \left(\frac{2c_n}{c^3}\right) n + \left(\frac{6(c_n)^2}{c^4} - \frac{2c_{nn}}{c^3}\right)\frac{n^2}{2} + \cdots$$

and

$$\frac{1}{h^2} = 1 - \left(\frac{2h_n}{h^3}\right) n + \left(\frac{6(h_n)^2}{h^4} - \frac{2h_{nn}}{h^3}\right)\frac{n^2}{2} + \cdots .$$

After rewriting these equations in terms of $\nu = \omega^{1/2} n$ and substituting for the coefficient of ω^2 in (A5), we obtain

$$\omega\left\{\left[-\left(\frac{c_{nn}}{c^3}\right)\nu^2 + O(\omega^{-1/2})\right] + \frac{ic_s}{(hc^2)} U - \frac{i}{c}\left(\frac{1}{h}\right)_s U - \frac{2i}{hc} U_s + hU_{\nu\nu} - \frac{ir_s}{rhc} U\right\} + \omega^{1/2}\left(U_\nu h_n + \frac{r_n h}{r} U_\nu\right) + \frac{1}{h} U_{ss} + U_s\left(\frac{1}{h}\right)_s + \frac{r_s}{rh} U_s = 0 . \quad \text{(A6)}$$

We now seek a solution of Eq. (A6) in the form

$$U(s,\nu,\omega) = U^0 + U^1/\omega^{1/2} + U^2/\omega + \cdots .$$

Then, to $O(\omega)$, one obtains

$$\left[-\left(\frac{c_{nn}}{c^3}\right)\nu^2 + \frac{ic_s}{c^2} - \frac{ir_s}{rc}\right] U^0 - \frac{2i}{c} U^0_s + U^0_{\nu\nu} = 0 . \quad \text{(A7)}$$

The final form of the ray-centered parabolic wave equation is obtained after introducing $W(s,\nu)$, defined by

$$U^0(s,\nu) = W(s,\nu)\sqrt{(c(s)/r)} . \quad \text{(A8)}$$

This gives

$$-(2i/c) W_s + W_{\nu\nu} - (\nu^2 c_{nn}/c^3) W = 0 , \quad \text{(A9)}$$

which is equivalent to Eq. (11) of Ref. 12. We observe, however, that the resulting $u(s,n)$ differs by a factor of $\sqrt{r}$, representing the effect of cylindrical spreading. In particular, combining Eqs. (A3) and (A8), we obtain

$$u(s,n) = \sqrt{\frac{c(s)}{r}} \exp\left(-i\omega \int \frac{ds}{c(s)}\right) W(s,\nu) . \quad \text{(A10)}$$

It remains to solve the equation for $W(s,\nu)$. The remainder of the analysis is identical with that of Cerveny *et al.*[12] We seek

$$W(s,\nu) = A(s)\exp[-i\nu^2\Gamma(s)/2] \quad \text{(A11)}$$

and obtain

$$-i(2A_s/c + A\Gamma) - A\nu^2(\Gamma_s/c + \Gamma^2 + c_{nn}/c^3) = 0 .$$

Since this equation must be satisfied for all ν, the terms in parentheses must both vanish. Thus

$$2A_s/c + A\Gamma = 0 , \quad \text{(A12)}$$

$$\Gamma_s/c + \Gamma^2 + c_{nn}/c^3 = 0 . \quad \text{(A13)}$$

Equations (A12) and (A13) may be solved numerically to yield $W(s,\nu)$ and, therefore, the beam $u(s,n)$. Some additional manipulations are, however, useful in order to obtain linear equations. One advantage of doing so is that a pair of linearly independent solutions can be computed and then initial conditions can be changed without recalculating $A(s)$ and $\Gamma(s)$. The equation for Γ is a simple Ricatti equation, which may be reduced by standard techniques to a pair of first-order linear equations. One obtains

$$\Gamma(s) = p/q , \quad \text{(A14)}$$

where

$$q_s = cp ,$$

$$p_s = -c_{nn} q/c^2 . \quad \text{(A15)}$$

In terms of p and q one may easily check that

$$A(s) = A_0\sqrt{q(s)} , \quad \text{(A16)}$$

where A_0 is an arbitrary constant. Combining (A10), (A14), and (A16), one may represent the beam as

$$u(s,n) = A_0\sqrt{c(s)/[rq(s)]} \times \exp\{-i\omega[\tau(s) + 0.5[p(s)/q(s)]n^2]\} , \quad \text{(A17)}$$

where $p(s)$, $q(s)$, and $\tau(s)$ are defined by Eqs. (A15) and (A3). The quantity A_0 remains arbitrary, reflecting the linearity of the Helmholtz equation. Finally, as observed by Cerveny *et al.*,[12] the general solution of (A9) is known in terms of products of Hermite polynomials and Gaussians, which form a family of beam modes. Higher-order beam modes may optionally be included in the expansion of a point source.

APPENDIX B: SOLUTION OF THE *p–q* EQUATIONS IN AN n^2-LINEAR DOMAIN

Let (r_0, z_0) denote the coordinates of the beam origin and c_0 the sound speed at that point. Without loss of generality we pick a coordinate system such that the sound-speed gradient is parallel to the z axis. Then, defining $n(z) = c_0/c(z)$, we have by assumption,

$$n^2(z) = a + bz \quad \text{(B1)}$$

and $n(z_0) = 1$, where a and b are arbitrary constants. We also denote the initial takeoff angle by α. The central axis of the beam follows the conventional ray equations, which in this environment (n^2 linear) are well known to generate parabolic trajectories. One obtains

$$z(r)[b/(4\cos^2\alpha)](r - r_0)^2 + (\tan\alpha)(r - r_0) + z_0 , \quad \text{(B2)}$$

which one may quickly check gives the correct depth z_0 for the range r_0 and also has the correct slope of $\tan\alpha$ at this point.

The p–q equations admit two linearly independent solutions. Our starting point is the representation obtained by Madariaga[22] in general stratified environments. One solution is obtained by inspection;

$$q_1 = \sin\theta\,, \tag{B3}$$

where θ is the ray angle at any point in the medium. At times we shall leave results in terms of the ray angle, remembering that at an arbitrary (r,z) the index of refraction may be computed and then the angle is determined by Snell's law:

$$n(z)\cos\theta = \cos\alpha\,. \tag{B4}$$

Knowing q_1, the corresponding p_1 is obtained by differentiation. Recall that

$$p = \frac{1}{c}\frac{dq}{ds} = \frac{n}{c_0}\frac{dq}{ds} = \frac{n}{c_0}\frac{dq}{dr}\frac{dr}{ds}\,. \tag{B5}$$

Since $\partial n/\partial r = 0$ one obtains from the ray equations $\rho = \cos\alpha$ and then

$$\frac{dr}{ds} = \frac{\cos\alpha}{n}\,. \tag{B6}$$

Thus

$$p = \frac{n}{c_0}\frac{dq}{dr}\frac{\cos\alpha}{n} = \frac{\cos\alpha}{c_0}\frac{dq}{dr} \tag{B7}$$

and

$$p_1 = \frac{\cos\alpha}{c_0}\frac{dq}{d\theta}\frac{d\theta}{dr} = \frac{\cos\alpha}{c_0}\cos\theta\frac{d\theta}{dr}\,. \tag{B8}$$

Differentiating Snell's law, one obtains

$$\frac{d\theta}{dr} = \frac{dn}{dr}\frac{\cos\theta}{n\sin\theta}\,. \tag{B9}$$

Also, differentiating $n^2 = a + bz$ gives $2n\,dn/dr = b\,dz/dr$ and so

$$\frac{dn}{dr} = \frac{b}{2n}\frac{dz}{dr}\,, \tag{B10}$$

which implies

$$\frac{d\theta}{dr} = \frac{b}{2n^2}\cot\theta\frac{dz}{dr}\,. \tag{B11}$$

Substituting in (B8), one finally obtains

$$\begin{aligned} p_1 &= \frac{\cos\alpha}{c_0}\cos\theta\frac{b}{2n^2}\cot\theta\frac{dz}{dr} \\ &= 0.5\frac{b}{c_0}\frac{dz}{dr}\frac{\cos^3\alpha}{n^4\sin\theta}\,. \end{aligned} \tag{B12}$$

A second linearly independent solution is obtained by reduction of order. One finds[22]

$$q_2 = f\sin\theta\,, \tag{B13}$$

where f satisfies

$$\frac{df}{dz} = \frac{c_0}{n(z)\sin^3\theta}\,, \tag{B14}$$

or

$$\frac{df}{d\theta}\frac{d\theta}{dz} = \frac{c_0}{n(z)\sin^3\theta}\,. \tag{B15}$$

As before, one invokes the differentiated Snell's law

$$\theta_z = b\cos\theta/(2n^2\sin\theta)\,, \tag{B16}$$

which is substituted in (B15) to give

$$\frac{df}{d\theta} = \frac{2c_0 n}{b\cos\theta\sin^2\theta} = \frac{2c_0\cos\alpha}{b\cos^2\theta\sin^2\theta}\,. \tag{B17}$$

Equation (B17) is integrated to obtain

$$f(\theta) = [(1-2\cos^2\theta)/(\cos\theta\sin\theta)]2c_0\cos\alpha/b \tag{B18}$$

and so,

$$\begin{aligned} q_2 &= (2c_0\cos\alpha/b)(1-2\cos^2\theta)/\cos\theta \\ &= (2c_0/b)\,(n - 2\cos^2\alpha/n)\,. \end{aligned} \tag{B19}$$

Again, the corresponding $p(s)$ is obtained by differentiation. Recalling (B7),

$$\begin{aligned} p_2 &= \frac{\cos\alpha}{c_0}\frac{dq_2}{dr} \\ &= \frac{\cos\alpha}{c_0}\left(\frac{2c_0}{b}\right)\left(\frac{d(n-2\cos^2\alpha/n)}{dn}\right)\left(\frac{dn}{dr}\right) \\ &= \cos\alpha\left(1+\frac{2\cos^2\alpha}{n^2}\right)\frac{1}{n}\frac{dz}{dr}\,. \end{aligned} \tag{B20}$$

In summary, the general p,q solution has the form

$$p = Ap_1 + Bp_2,\quad q = Aq_1 + Bq_2 \tag{B21}$$

where

$$\begin{aligned} p_1 &= \left(\frac{b\,dz/dr}{2c_0}\right)\frac{\cos^3\alpha}{n^4\sin\theta}\,, \\ q_1 &= \sin\theta\,, \\ p_2 &= \frac{dz}{dr}\cos\alpha\left(\frac{1}{n}+\frac{2\cos^2\alpha}{n^3}\right), \\ q_2 &= (2c_0/b)(n-2\cos^2\alpha/n)\,, \end{aligned} \tag{B22}$$

and, of course, $dz/dr = [b/(2\cos^2\alpha)](r - r_0) + \tan\alpha$.

[1] G. A. Deschamps and P. E. Mast, "Beam tracing and applications," *Quasi-Optics* (Polytechnic, Brooklyn, 1964), pp. 379–395.

[2] P. K. Tien, J. P. Gordon, and J. R. Whinnery, "Focusing of a light beam of Gaussian field distribution in continuous and periodic lens-like media," Proc. IEEE **53**, 129–136 (1965).

[3] H. Kogelnik, "On the propagation of Gaussian beams of light through lenslike media including those with a loss or gain variation," Appl. Opt. **4**, 1562–1569 (1965).

[4] J. B. Keller and W. Streifer, "Complex rays with an application to Gaussian beams," J. Opt. Soc. Am. **61**, 40–43 (1971).

[5] G. A. Deschamps, "Gaussian beam as a bundle of complex rays," Elec. Lett. 7(23), 684–685 (1971).

[6] L. B. Felsen, "Evanescent waves," J. Opt. Soc. Am. **66**(8), 751–760 (1976).

[7] M. M. Popov and I. Psencik, "Computation of ray amplitudes in inhomogenous media with curved interfaces," Studia Geophys. Geod. **22**, 248–258 (1978).

[8] M. M. Popov, "A method of calculating the geometric divergence in an inhomogeneous medium with interfaces," Dok. Akad. Nauk SSSR **237**, 40–42 (1980).

[9] A. P. Kachalov and M. M. Popov, "Application of the method of summa-

tion of Gaussian beams for calculation of high-frequency wave fields," Sov. Phys. Dokl. **26**(6), 604–606 (1981).
[10]V. M. Babich and M. M. Popov, "Propagation of concentrated sound beams in a three-dimensional inhomogeneous medium," Sov. Phys. Acoust. **27**(6), 459–462 (1982).
[11]M. M. Popov, "A new method of computation of wave fields using Gaussian beams," Wave Mot. **4**, 85–97 (1982).
[12]V. Cerveny, M. M. Popov, and I. Psencik, "Computation of wave fields in inhomogeneous media—Gaussian beam approach," Geophys. J. R. Astron. Soc. **70**, 109–128 (1982).
[13]V. E. Grikurov and M. M. Popov, "Summation of Gaussian beams in a surface waveguide," Wave Motion **5**, 225–233 (1983).
[14]V. Cerveny and I. Psencik, "Gaussian beams in two-dimensional elastic inhomogeneous media," Geophys. J. R. Astron. Soc. **72**, 417–433 (1983).
[15]V. Cerveny, "Synthetic body wave seismograms for laterally varying layered structures by the Gaussian beam method," Geophys. J. R. Astron. Soc. **73**, 389–426 (1983).
[16]R. Nowack and K. Aki, "The two-dimensional Gaussian beam synthetic method: testing and applications," J. Geophys. Res. **89**, 7797–7819 (1984).
[17]V. Cerveny and I. Psencik, "Gaussian beams in elastic 2-D laterally varying layered structures," Geophys. J. R. Astron. Soc. **78**, 65–91 (1984).
[18]L. B. Felsen, "Geometrical theory of diffraction, evanescent waves, complex rays and Gaussian beams," Geophys. J. R. Astron. Soc. **79**, 77–88 (1984).
[19]L. Klimes, "Expansion of a high-frequency time-harmonic wavefield given on an initial surface into Gaussian beams," Geophys. J. R. Astron. Soc. **79**, 105–118 (1984).
[20]V. Cerveny and L. Klimes, "Synthetic body wave seismograms for three-dimensional laterally varying media," Geophys. J. R. Astron. Soc. **79**, 119–133 (1984).
[21]G. Muller, "Efficient calculation of Gaussian-beam seismograms for two-dimensional inhomogeneous media," Geophys. J. R. Astron. Soc. **79**, 153–166 (1984).
[22]R. Madariaga, "Gaussian beam synthetic seismograms in a vertically varying medium," Geophys. J. R. Astron. Soc. **79**, 589–612 (1984).
[23]H. P. Bucker and M. B. Porter, "Gaussian beams and 3-D bottom interacting acoustic systems," in *Ocean Seismo-Acoustics*, edited by T. Akal and J. Berkson (Plenum, New York, 1986).
[24]A. P. Katchalov and M. M Popov, "Application of the Gaussian beam method to elasticity theory," Geophys. J. R. Astron. Soc. **81**, 205–214 (1985).
[25]A. Ben-Menahem, B. Ben-Menahem, and B. Wafik, "Range of validity of seismic ray and beam methods in general inhomogeneous media—I. General theory," Geophys. J. R. Astron. Soc. **82**, 207–234 (1985).
[26]K. Yomogida and K. Aki, "Waveform synthesis of surface waves in a laterally heterogeneous earth by the Gaussian beam method," J. Geophys. Res. **90**, 7665–7668 (1985).
[27]R. Wu, "Gaussian beams, complex rays, and the analytic extension of the Green's function in smoothly inhomogeneous media," Geophys. J. R. Astron. Soc. **83**, 93–110 (1985).
[28]S. Ramo, J. R. Whinnery, and T. Van Duzer, *Fields and Waves in Communication Electronics* (Wiley, New York, 1984), pp. 768–778.
[29]L. Collatz, *The Numerical Treatment of Differential Equations* (Springer, New York, 1966).
[30]M. A. Pedersen and D. F. Gordon, "Normal-mode and ray theory applied to underwater acoustic conditions of extreme downward refraction," J. Acoust. Soc. Am. **51**, 323–368 (1972).
[31]H. W. Kutschale, "Rapid computation by wave theory of propagation loss in the arctic ocean," Lamont-Doherty Geophys. Observ. Columbia U. Tech. Rep. CU-8-73 (1973).
[32]W. H. Munk, "Sound channel in an exponentially stratified ocean with applications to SOFAR," J. Acoust. Soc. Am. **55**, 220–226 (1974).
[33]M. B. Porter and E. L. Reiss, "A numerical method for ocean acoustic normal modes," J. Acoust. Soc. Am. **76**, 224–252 (1984).
[34]F. B. Hildebrand, *Advanced Calculus for Applications* (Prentice-Hall, Englewood Cliffs, NJ, 1976), pp. 306–311.